Structural phases driven by oxygen vacancies at the La0.7Sr0.3MnO3/SrTiO3 hetero-interface

M. Nord, P. E. Vullum, M. Moreau, J. E. Boschker, S. M. Selbach, R. Holmestad, and T. Tybell

Citation: Applied Physics Letters **106**, 041604 (2015); doi: 10.1063/1.4906920
View online: http://dx.doi.org/10.1063/1.4906920
View Table of Contents: http://scitation.aip.org/content/aip/journal/apl/106/4?ver=pdfcov
Published by the AIP Publishing

Structural phases driven by oxygen vacancies at the $La_{0.7}Sr_{0.3}MnO_3/SrTiO_3$ hetero-interface

M. Nord,[1] P. E. Vullum,[1,2] M. Moreau,[3] J. E. Boschker,[3] S. M. Selbach,[4] R. Holmestad,[1] and T. Tybell[3,a)]
[1]*Department of Physics, NTNU, 7491 Trondheim, Norway*
[2]*Materials and Chemistry, SINTEF, 7465 Trondheim, Norway*
[3]*Department of Electronics and Telecommunications, NTNU, 7491 Trondheim, Norway*
[4]*Department of Materials Science and Engineering, NTNU, 7491 Trondheim, Norway*

(Received 12 October 2014; accepted 17 January 2015; published online 29 January 2015)

An oxygen vacancy driven structural response at the epitaxial interface between $La_{0.7}Sr_{0.3}MnO_3$ films and $SrTiO_3$ substrates is reported. A combined scanning transmission electron microscopy and electron energy loss spectroscopy study reveal the presence of an elongated out-of-plane lattice parameter, coupled to oxygen vacancies and reduced manganese oxidation state at the $La_{0.7}Sr_{0.3}MnO_3$ side of the interface. Density functional theory calculations support that the measured interface structure is a disordered oxygen deficient brownmillerite structure. The effect of oxygen vacancy mobility is assessed, revealing an ordering of the vacancies with time. © *2015 AIP Publishing LLC*. [http://dx.doi.org/10.1063/1.4906920]

Perovskite oxide materials exhibit interesting magnetic, electric, dielectric, and piezoelectric properties, which make them a promising and important class of functional materials. For example, $La_{0.7}Sr_{0.3}MnO_3$ (LSMO) is a mixed-valence system where the interplay between Mn^{+3} and Mn^{+4} gives properties such as colossal magnetoresistance through double-exchange.[1] In particular, the LSMO/$SrTiO_3$ (STO) heterostructure has been considered a promising system for devices such as magneto-tunneling junctions, metal-based spintronics, and magnetic memory. A recent development is the fabrication of oxygen-poor modulations of the perovskite structure as thin films. Ferguson *et al.*[2] induced oxygen vacancies in LSMO grown on STO, using a top layer of oxygen deficient STO as an oxygen getter. This resulted in a brownmillerite phase, where the oxygen vacancies ordered into a superstructure. Similar structures have also been reported in $La_{0.5}Sr_{0.5}CoO_{3-\delta}$ (LSCO) heterostructures. Growing the LSCO on substrates with different lattice mismatch led to different kinds of oxygen vacancy ordering, driven by strain relief accommodation.[3] These structures are not only interesting for the ionic transport[4] properties but also for their effect on other functional properties. *Ab-initio* calculations predict oxygen vacancies close to the interface of tensilely strained films.[5] There have also been several observations of changes in cation oxidation state[6–8] and lattice parameter[9] close to interfaces in similar systems. Understanding the correlation between oxygen vacancies and B-site cation oxidation state, and how the oxygen vacancies behave and order over time is important for implementation in devices.

In this letter, we report on a combined Scanning Transmission Electron Microscopy-Electron Energy Loss Spectroscopy (STEM-EELS) and Density Functional Theory (DFT) study of a LSMO/STO heterostructure, where a coupling between oxygen vacancies, the manganese oxidation state, and an elongated out-of-plane lattice parameter in the LSMO film close to the interface is observed. We attribute these observations to a brownmillerite structure with disordered oxygen vacancies, which order over time.

35 nm thick epitaxial LSMO films were grown on (001)-oriented STO substrates using pulsed laser deposition and *in-situ* RHEED analysis.[10] The substrates were annealed for 1 h at 950 °C in oxygen ambient before the deposition. A KrF excimer laser ($\lambda = 248$ nm) with a fluency of $\sim 2\ J\ cm^{-2}$ and a repetition rate of 1 Hz was employed on a stoichiometric $La_{0.7}Sr_{0.3}MnO_3$ target.[10] Cross sectional TEM foils were prepared using mechanical tripod wedge polishing followed by low-energy Ar-ion milling. A combined STEM-EELS and STEM-high angle angular dark field (HAADF) study was performed to probe the electronic and lattice structure at the interface using a probe corrected FEI Titan 80–300, with a beam energy of 300 keV. The energy resolution of EELS was found to be 1.0 eV from the full width at half maximum (FWHM) of the zero loss peak. The STEM and EELS study on the ordered brownmillerite after 1.5 years was performed on a probe- and image-corrected cold-FEG Jeol ARM 200F. For the EELS analysis, principal component analysis (PCA)[11] was used to reduce noise and standard power law background subtraction was done using HyperSpy.[12] To increase the electron count statistics, the EELS data were not collected at atomic resolution, but with a larger probe. To rule out the effect of the electron beam inducing changes in the material, the same EELS experiments were performed in similar regions with shorter exposure and at a beam energy of 120 keV, showing the same results as the 300 keV data at 3 s exposure time. In addition, electron beam exposure tests were performed, where the same area was exposed to the electron beam for 30 s under the same experimental conditions as the data in this work. No significant changes in the EELS data were observed. The DFT calculations were done with the Projector Augmented Wave (PAW) method[13] as

a)Author to whom correspondence should be addressed. Electronic mail: thomas.tybell@iet.ntnu.no

implemented in the Vienna *Ab-initio* Simulation Package (VASP),[14,15] using the PBEsol functional[16] with a GGA + U approximation.[17] The La, Sr_sv, Mn_sv, and standard O PBE PAW potentials supplied with VASP were used, and a Hubbard U correction of 3 eV and 10 eV was applied to the Mn 3d electrons and La 4f orbitals, respectively, in concordance with previous related investigations.[5,18] A 36 atom $La_6Sr_2Mn_8O_{20}$ unit cell with a $6 \times 6 \times 2$ gamma centered k-point mesh and a plane wave cutoff energy of 550 eV was used for the calculations of the oxygen deficient LSMO unit cells. The in-plane lattice constants were fixed at the equilibrium calculated value for cubic STO, while the ionic coordinated and out-of-plane lattice constant were allowed to relax until the Hellmann-Feynman forces on the ions were smaller than 0.01 eV/Å.

The structural quality of the thin film and substrate was investigated by STEM-HAADF. Fig. 1(a) shows typical data, revealing a coherent interface, and X-ray analysis confirms that the films are epitaxial.[10]

Possible strain around the epitaxial interface was analyzed relying on geometrical phase analysis (GPA)[19] of the STEM-HAADF data. Fig. 1(a) shows a STEM-HAADF image of the LSMO/STO heterostructure, and the corresponding out-of-plain strain data from GPA is displayed in Fig. 1(b). Using the lattice parameter of bulk STO, 3.905 Å, as a reference, the substrate averages as expected to 0% out-of-plane strain, with a standard deviation of 0.17%. For the film, an elongated out-of-plane lattice parameter is observed in the first 3 nm. This corresponds to a relative out-of-plane strain of 2.5% compared to the LSMO bulk pseudo cubic lattice parameter of 3.876 Å. Similar strain has been reported in BFO grown on LSMO/STO,[9] where the first few unit cells closest to the interface are elongated in the out-of-plane direction.

To further investigate the region with enlarged out-of-plane LSMO lattice parameter, we probe the electronic structure by EELS, providing information on both the manganese and oxygen electronic state through the Mn-$L_{2,3}$ and O-K core loss edges. EELS line scans were acquired in a line orthogonal to the film/substrate interface, as schematically shown in Fig. 2(a), with STEM-EELS data representative for (i) the bulk LSMO film (red), (ii) the interface on the film side (green), and (iii) the bulk STO (blue), presented in Fig. 2(b). The manganese edge consists of two peaks: L_3 (Mn

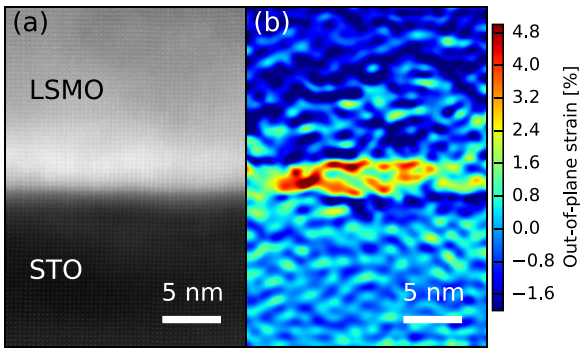

FIG. 1. (a) Cross-sectional STEM-HAADF image of the LSMO/STO heterostructure, showing a coherent interface. (b) Map of the out-of-plane strain in (a), using the STO-substrate (3.905 Å) as a reference.

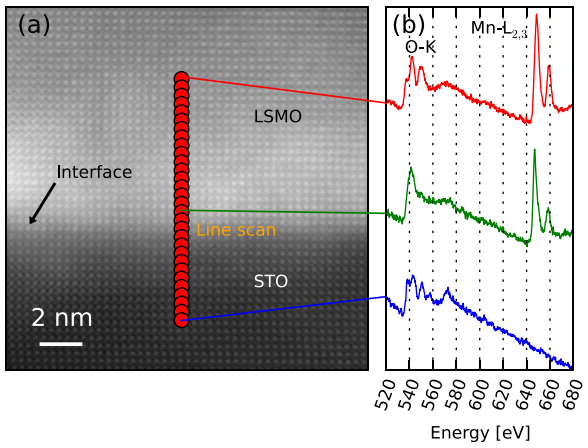

FIG. 2. (a) Cross-sectional STEM-HAADF image of the LSMO/STO heterostructure. (b) Results of an EELS line scan across the LSMO/STO interface.

$2P_{3/2} \rightarrow 3d$) and L_2 (Mn $2P_{1/2} \rightarrow 3d$),[11] see Fig. 3(a). There is a clear difference between the Mn-$L_{2,3}$ spectra acquired at the interface and those acquired away from the interface. The intensity ratio between the L_3 and L_2 peaks (L_3/L_2-ratio)

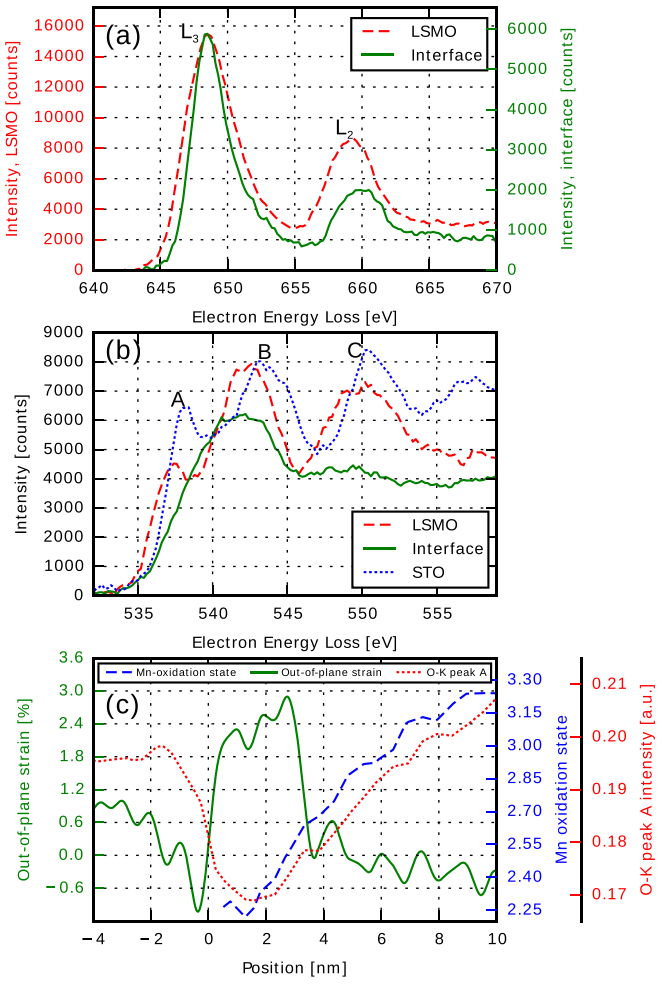

FIG. 3. (a) Manganese L_2- and L_3-edges from the middle of the LSMO film, and LSMO film side of the interface. (b) Oxygen K-edge from the LSMO film side of the interface, in the middle of the LSMO film, and STO substrate. (c) Integrated out-of-plane strain from Fig. 1(b), manganese oxidation state and integrated oxygen K-edge peak A intensity normalized on the total O-K edge intensity (shown in Fig. 3(b)).

is larger at the interface. This is indicative of a lower Mn oxidation state at the interface as compared to bulk LSMO, as the intensity of the L_3 peak increases relative to the L_2 peak when the Mn oxidation state is lowered.[11,20] We note that the FWHM line width of the Mn-L_3 peak is smaller at the interface as compared to the rest of the film, supporting a lower Mn oxidation state at the interface.[20] The Mn-oxidation state was estimated as in Varela *et al.*[11] and plotted in Fig. 3(c) (blue dashed line). As can be seen in Fig. 3(c), a clear trend for the Mn oxidation state was observed: starting at 3.2 far from the interface and monotonically decreasing towards 2.3 close to the interface. This trend of a reduction in Mn oxidation state has also been observed in (La,Ca)MnO_3/STO[6] and $TbMnO_3$/STO,[7] and has been proposed to explain the observed magnetic "dead layer" in similar systems.[21]

In order to investigate the possible presence of oxygen vacancies, known to be present in similar thin film systems,[2] the oxygen electronic structure was investigated. As seen in Fig. 2(b), large spectral differences are observed between the oxygen K-edges across the interface. The oxygen K-edges from the (i) middle of the film, (ii) film side of the interface, and (iii) STO bulk are shown in detail in Fig. 3(b). The main fine structure peaks are labeled as A, B, and C. The O-K edges from the bulk of the film, and the STO substrate, are consistent with LSMO[8] and STO bulk[22] data previously reported. However, the O-K edge at the LSMO side of the interface is not consistent with LSMO bulk. We observe that peak A is weak or not present in the LSMO interface region. Peak A is attributed to the covalent interaction between O 2p and Mn 3d states in the LSMO perovskite structures,[11] and is known to be sensitive to the Mn oxidation state. In addition, a weakening of peaks A and C in conjunction with a broadening of peak B has been correlated with oxygen vacancies.[23] The bond between Mn and O becomes more ionic as the Mn oxidation state decreases, reducing the interaction between the orbitals. A low Mn oxidation state then corresponds to a less intense peak,[11] consistent with the Mn L-edge data. We take the integrated intensity of peak A normalized over the total O-K intensity as a measure of oxygen content, the results of this shown in Fig. 3(c) (red dotted line). As can be seen, the amount of oxygen vacancies increases towards the interface, and subsequently decreases to a constant value in the substrate.

The strain, shift in Mn oxidation state and the changes in oxygen signal imply a deviation from the perovskite structure at the film side of the interface. The formal valence for Mn in $La_{0.7}{}^{+3}$ $Sr_{0.3}{}^{+2}Mn^{+3.3}O_3{}^{-2}$ (valence shown in superscript) is 3.3. Removing oxygen lowers the Mn oxidation state as the charge compensating electrons localize on Mn, consistent with the data. We note that oxygen vacancies can be expected close to the interface in thin films that are tensiled strained by the substrate.[5] Assuming that the whole shift in Mn oxidation state is due to oxygen vacancies, an oxygen deficiency of $\delta = 0.5$ ($LSMO_{3-\delta}$) is found (corresponding to $La_{0.7}Sr_{0.3}MnO_{2.5}$). This amount of oxygen vacancies is also consistent with the oxygen fine structure, which is similar to the one reported by Yao *et al.*[23] This large number of oxygen vacancies breaks the MnO_6 octahedron, and hence, destroys the perovskite structure.[24] A known cation non-stoichiometric phase is the Ruddlesden-Popper structure.[25] However, our high-resolution STEM-HAADF data are not consistent with the clear signature of such a phase. Other cation non-stoichiometries, such as La- or Mn- deficient phases, correspond to an increase in the formal Mn valence, not consistent with our EELS data. A possible reduction in Sr-content would lower the Mn oxidation state, however, this is not consistent with the O-K edge.[26] Therefore, we do not attribute the observed changes to cation non-stoichiometry.

The oxygen deficient brownmillerite structure, $ABO_{2.5}$ is compatible with the experimental data. Recently, there have been several reports on thin film synthesis of brownmillerites in multiple material systems.[2,27–29] For example, a brownmillerite phase, where oxygen vacancies are ordered, was shown in a LSMO/STO heterostructure by Ferguson *et al.*[2] In that work, the vacancies were ordered in preferred layers resulting in an out-of-plane lattice parameter of 16.47 Å, corresponding to four pseudo-cubic LSMO unit cells with a 6.1% elongation of the out-of-plane lattice parameter compared to the stoichiometric perovskite. This is considerably larger than the 2.5% elongation we measure close to the interface in this work. However, one possibility is that disordered oxygen vacancies result in a lower out-of-plane strain state. In order to test this hypothesis, we have performed DFT calculations on brownmillerites with ordered and disordered oxygen vacancy structures. The calculations were performed on structures with different oxygen vacancy positions (see supplementary material[30]), the results shown in Table I. There is a clear trend that structures with oxygen vacancies ordered in layers are more stable than oxygen vacancies distributed in all the Mn layers. The most stable structure, corresponding to the one observed by Ferguson *et al.*,[2] is 0.223 eV/f.u. more stable than the most stable disordered structure. However, the DFT calculations also reveal that the disordered structures all show an elongated out-of-plane lattice parameter in the order of 1%–2%, in good agreement with our experimental strain data, while the ordered structures show an elongation in the order of 6%–7%.

TABLE I. DFT calculated energy differences between the different oxygen vacancy brownmillerite structures and the most stable ordered structure, given per $ABO_{2.5}$ formula unit, and the corresponding out-of-plane strain compared to stoichiometric bulk LSMO. The different structures (A, B, C, and D) referring to different positioning of the oxygen vacancies, see supplementary material[30] for details.

	Ordered structure A	Ordered structure B	Ordered structure C	Disordered structure A	Disordered structure B	Disordered structure C	Disordered structure D
ΔE/f.u. (eV)	0.014	0	0.035	0.304	0.357	0.223	0.238
Strain (%)	6.72	6.52	7.00	2.38	2.39	1.55	2.11

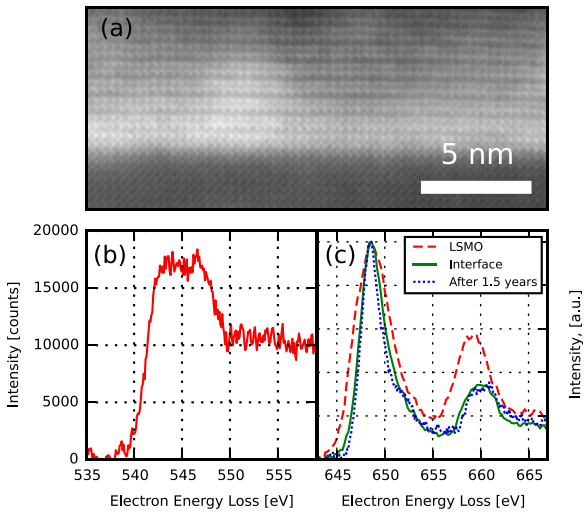

FIG. 4. (a) Cross sectional STEM-HAADF image from the same TEM lamella as Figs. 1(a) and 2(a), after approximately 1.5 years showing an ordered brownmillerite superstructure at the film side of the interface. (b) Representative STEM-EELS data from the superstructure in (a), showing an oxygen K-edge consistent with oxygen vacancies. (c) The same as (b) but for the Mn-$L_{2,3}$ edge, with the spectra from Fig. 3(a) as comparison.

Based on the above discussion, a brownmillerite phase with disordered oxygen vacancies at the LSMO side of the interface towards STO is the only interpretation that agrees with both STEM and EELS data and DFT calculations. Fig. 4(a) shows STEM-HAADF data taken on the same TEM lamellas after approximately 1.5 years. Here, we find an ordered, layered structure at the interface, compatible with an ordered brownmillerite phase.[2] Figs. 4(b) and 4(c) display representative O-K and Mn-$L_{2,3}$ EELS edges from the ordered structure, confirming the presence of oxygen vacancies and manganese oxidation state corresponding to the one observed close to the interface in the disordered phase. GPA of the layered structure reveals an elongated lattice parameter of 5%–6% compared to LSMO bulk, consistent with the DFT-calculations. However, just at the interface a larger elongation is observed. This ordering of the oxygen vacancies with time is in agreement with the ~0.2 eV energy difference between the ordered and disordered structures found using DFT.

In conclusion, we have studied the strain and electronic structure of a LSMO/STO heterojunction using STEM-HAADF and STEM-EELS. The results reveal a region with an elongated out-of-plane lattice parameter, reduced oxygen content, and lowered manganese oxidation state extending from the interface to about 3 nm into the LSMO film. These properties are attributed to the presence of a brownmillerite phase with disordered oxygen vacancies, in agreement with DFT calculations, not previously reported in as-grown LSMO/STO thin films. After approximately 1.5 years, the same TEM lamella show a brownmillerite phase with ordered oxygen vacancies. These finding shed light on the effect of oxygen vacancies on the structure of complex perovskite oxide interfaces, and reveal that they can order over time possibly affecting functional properties.

This project was supported by the Norwegian Research Council under Project No. 10239707 and The Norwegian PhD Network on Nanotechnology for Microsystems. Takeshi Kasama at Center for Electron Nanoscopy at the Technical University of Denmark (CEN-DTU) was thankfully acknowledged for support with the STEM-EELS investigations. The Norwegian Metacenter for Computational Science (Notur) was acknowledged for providing computational resources for DFT-calculations through the project NN9301K.

[1]Y. Tokura, Rep. Prog. Phys. **69**, 797 (2006).
[2]J. D. Ferguson, Y. Kim, L. F. Kourkoutis, A. Vodnick, A. R. Woll, D. A. Muller, and J. D. Brock, Adv. Mater. **23**, 1226 (2011).
[3]J. Gazquez, S. Bose, M. Sharma, M. A. Torija, S. J. Pennycook, C. Leighton, and M. Varela, APL Mater. **1**, 012105 (2013).
[4]S. V. Kalinin and N. A. Spaldin, Science **341**, 858 (2013).
[5]U. Aschauer, R. Pfenninger, S. M. Selbach, T. Grande, and N. A. Spaldin, Phys. Rev. B **88**, 054111 (2013).
[6]A. Kobrinskii, A. Goldman, M. Varela, and S. Pennycook, Phys. Rev. B **79**, 094405 (2009).
[7]S. Venkatesan, M. Döblinger, C. Daumont, B. Kooi, B. Noheda, J. T. M. De Hosson, and C. Scheu, Appl. Phys. Lett. **99**, 222902 (2011).
[8]L. Samet, D. Imhoff, J.-L. Maurice, J.-P. Contour, A. Gloter, T. Manoubi, A. Fert, and C. Colliex, Eur. Phys. J. B: Condens. Matter **34**, 179 (2003), available at http://link.springer.com/article/10.1140%2Fepjb%2Fe2003-00210-8.
[9]A. Y. Borisevich, H. J. Chang, M. Huijben, M. P. Oxley, S. Okamoto, M. K. Niranjan, J. D. Burton, E. Y. Tsymbal, Y. H. Chu, P. Yu *et al.*, Phys. Rev. Lett. **105**, 087204 (2010).
[10]J. E. Boschker, E. Folven, Å. F. Monsen, E. Wahlström, J. K. Grepstad, and T. Tybell, Cryst. Growth Des. **12**, 562 (2012).
[11]M. Varela, M. Oxley, W. Luo, J. Tao, M. Watanabe, A. Lupini, S. Pantelides, and S. Pennycook, Phys. Rev. B **79**, 085117 (2009).
[12]See http://hyperspy.org/ for HyperSpy: Hyperspectral data analysis toolbox.
[13]P. E. Blochl, Phys. Rev. B **50**, 17953 (1994).
[14]G. Kresse and D. Joubert, Phys. Rev. B **59**, 1758 (1999).
[15]G. Kresse and J. Furthmuller, Phys. Rev. B **54**, 11169 (1996).
[16]J. P. Perdew, A. Ruzsinszky, G. I. Csonka, O. A. Vydrov, G. E. Scuseria, L. A. Constantin, X. Zhou, and K. Burke, Phys. Rev. Lett. **100**, 136406 (2008).
[17]V. I. Anisimov, J. Zaanen, and O. K. Andersen, Phys. Rev. B **44**, 943 (1991).
[18]R. L. Johnson-Wilke, D. Marincel, S. Zhu, M. P. Warusawithana, A. Hatt, J. Sayre, K. T. Delaney, R. Engel-Herbert, C. M. Schlepütz, J.-W. Kim *et al.*, Phys. Rev. B **88**, 174101 (2013).
[19]M. J. Hÿtch, E. Snoeck, and R. Kilaas, Ultramicroscopy **74**, 131 (1998).
[20]T. Riedl, T. Gemming, and K. Wetzig, Ultramicroscopy **106**, 284 (2006).
[21]R. P. Borges, W. Guichard, J. G. Lunney, J. M. D. Coey, and F. Ott, J. Appl. Phys. **89**, 3868 (2001).
[22]D. A. Muller, N. Nakagawa, A. Ohtomo, J. L. Grazul, and H. Y. Hwang, Nature **430**, 657 (2004).
[23]L. Yao, S. Majumdar, L. Äkäslompolo, S. Inkinen, Q. H. Qin, and S. V. Dijken, Adv. Mater. **26**, 2789 (2014).
[24]S. Stølen, E. Bakken, and C. E. Mohn, Phys. Chem. Chem. Phys. **8**, 429 (2006).
[25]R. G. Palgrave, P. Borisov, M. S. Dyer, S. R. C. McMitchell, G. R. Darling, J. B. Claridge, M. Batuk, H. Tan, J. Verbeeck, J. Hadermann *et al.*, J. Am. Chem. Soc. **134**, 7700 (2012).
[26]A. B. Shah, Q. M. Ramasse, S. J. May, J. Kavich, J. G. Wen, X. Zhai, J. N. Eckstein, J. Freeland, A. Bhattacharya, and J. M. Zuo, Phys. Rev. B **82**, 115112 (2010).
[27]K. Matsumoto, M. Haruta, M. Kawai, A. Sakaiguchi, N. Ichikawa, H. Kurata, and Y. Shimakawa, Sci. Rep. **1**, 27 (2011).
[28]Y. M. Kim, J. He, M. D. Biegalski, H. Ambaye, V. Lauter, H. M. Christen, S. T. Pantelides, S. J. Pennycook, S. V. Kalinin, and A. Y. Borisevich, Nat. Mater. **11**, 888 (2012).
[29]H. Jeen, W. S. Choi, J. W. Freeland, H. Ohta, C. U. Jung, and H. N. Lee, Adv. Mater. **25**, 3651 (2013).
[30]See supplementary material at http://dx.doi.org/10.1063/1.4906920 for details on the different positioning of the oxygen vacancies in the simulated structures.